The impact of a storm on the microtidal flat in the Yellow River Delta

Yu, Haisheng; Xie, Weiming; Peng, Zhong; Xu, Fan; Sun, Jianwei; He, Qing

DOI
10.1016/j.ecss.2024.108978

Publication date
2024

Document Version
Final published version

Published in
Estuarine, Coastal and Shelf Science

Estuarine, Coastal and Shelf Science 311 (2024) 108978

Contents lists available at ScienceDirect

Estuarine, Coastal and Shelf Science

journal homepage: www.elsevier.com/locate/ecss

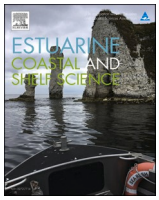

The impact of a storm on the microtidal flat in the Yellow River Delta

Haisheng Yu [a], Weiming Xie [a,*], Zhong Peng [a], Fan Xu [a], Jianwei Sun [a,b], Qing He [a]

[a] State Key Laboratory of Estuarine and Coastal Research, East China Normal University, Shanghai, 200241, China
[b] Faculty of Civil Engineering and Geosciences, Delft University of Technology, Stevinweg 1, Delft, 2628 CN, the Netherlands

ARTICLE INFO

Keywords:
Storm
Erosion
Recovery
Microtidal flat
Coastal protection

ABSTRACT

Strong hydrodynamic forces generated by storms are key in shaping coastal tidal flats. Most tidal flats achieve equilibrium by adapting to hydrodynamic conditions and sediment inputs. However, high-energy wave activity during storms disrupts this equilibrium, causing rapid and significant changes, particularly in tidal flats, especially in microtidal flats, which are characterized by low tidal ranges. In this study, we conducted an 11-d field campaign on a microtidal flat in the Yellow River Delta (YRD), capturing data during both stormy and calm weather conditions. We measured tidal currents, wave activity, suspended sediment concentrations and sediment grain sizes. The results demonstrated that the tidal flat maintained equilibrium under calm conditions, with minimal fluctuations in bed level (within ±2 mm). Contrastingly, severe erosion and sediment removal during the storm significantly altered the equilibrium of the area. The storm-induced high shear stresses, ranging from 1.02 to 1.48 N/m^2, along with alongshore sediment transport, resulted in an elevation change of −10 mm. Furthermore, the subsequent bed level recovery was minimal and insufficient to offset the erosion. Compared to that of the mesotidal and macrotidal flats, post-storm recovery on microtidal flats was limited due to shorter inundation periods and weaker hydrodynamic forces. Therefore, frequent storms may lead to continuous shoreline retreat on microtidal coasts. Conclusively, the present findings underscore the significant impact of storm-induced erosion on the evolutionary processes of microtidal flats and suggest that greater attention should be given to protecting these areas during storms in the Yellow River Delta. The insights can guide the development of more effective coastal protection strategies, highlighting the need for enhanced measures to mitigate erosion and promote resilience in microtidal regions.

1. Introduction

Tidal flats are frontier zones of land-sea interaction and serve as extensive habitats for a diverse array of invertebrates, fish, and birds, rendering them among the most valuable yet vulnerable ecosystems globally (Tognin et al., 2021). These coastal areas are increasingly subject to erosion and retreat due to factors, such as land reclamation, sea-level rise, diminished riverine sediment supply, and storm events (Kirwan and Megonigal, 2013; Leonardi et al., 2016). High-energy storms significantly alter tidal flat morphology, inducing morphological changes that can be 10–100 times greater than those observed under calm weather conditions (Leonardi et al., 2018). As climate change progresses, the frequency of extreme storms, particularly in the Pacific Northwest, is expected to rise sharply (Bacmeister et al., 2018), underscoring the significance of understanding tidal flat morphodynamics during such events for effective coastal defense.

Although numerous studies explored the impact of storms on the evolution of tidal flats, their findings have been inconsistent. Storms often cause substantial erosion, as bed shear stresses during these events exceed the critical shear stress for tidal flats, leading to significant erosion in a short period (van der Wegen et al., 2017; Xie et al., 2017; Yang et al., 2003). Contrastingly, the post-storm phase witnesses rapid recovery in certain cases, with sediment redeposition and elevation returning to pre-storm levels, particularly on mesotidal and macrotidal flats (Xie et al., 2017; Yang et al., 2003). Additionally, storms can resuspend sediment in adjacent seas, enhancing sediment supply to the intertidal zone and facilitating deposition on tidal flats (McKee and Cherry, 2009; Tognin et al., 2021; Xie et al., 2021). The morphological changes resulting from storms typically range from centimeters to decimeters (Fan et al., 2006; Siadatmousavi and Jose, 2015; Yang et al., 2003). However, the response of tidal flats to storms varies depending on factors, such as storms intensity, bed surface properties, and local environment. Earlier research predominantly focused on mesotidal and macrotidal flats, with insufficient comprehensive analysis of the

* Corresponding author.
E-mail address: wmxie@sklec.ecnu.edu.cn (W. Xie).

https://doi.org/10.1016/j.ecss.2024.108978
Received 22 March 2024; Received in revised form 6 September 2024; Accepted 2 October 2024
Available online 4 October 2024

combined effects of hydro-sedimentary dynamics and erosion intensity during storms on microtidal flats, which generally experience weaker hydrodynamics and shorter flooding durations than that in mesotidal and macrotidal flats (Christie et al., 2000; de Vet et al., 2020; Xie et al., 2017; Yang et al., 2003).

The majority of tidal flats in the Yellow River Delta (YRD) are situated in a microtidal environment, with a tidal range of less than 1.2 m. Prior research indicated that since 1996, the southern coastal region of the YRD has been experiencing ongoing erosion (Wang, 2019; Zhang et al., 2018). Nonetheless, during periods of fair weather, these tidal flats remained relatively stable due to the weak hydrodynamic forces and infrequent inundation events (Bi et al., 2021; Xie et al., 2021). This apparent contradiction between interannual erosion and stability under fair weather conditions presents a significant research challenge. Storms are crucial drivers of coastal erosion, as observed in the microtidal Mississippi Delta (Dietz et al., 2018). They frequently affect the YRD and are often accompanied by extratropical storms and cold fronts (Fan et al., 2020; Fu et al., 2021). Despite this, the impact of storm-induced erosion on shoreline erosion in the YRD is not extensively explored in earlier studies. Storm events are characterized by elevated water levels and strong hydrodynamic forces, which can cause significant erosion of tidal flats that dramatically alter their morphology in a short period (Isla et al., 2024; Niu et al., 2023; Pannozzo et al., 2023; Spiske et al., 2022; Xie et al., 2017; Yang et al., 2003). Thus, further research is necessary to understand the influence of short-term erosion on the long-term evolution of the YRD coastline.

In this study, field measurements were conducted to acquire hydrodynamic data, including currents, waves, and suspended sediment concentrations (SSC), in the southern region of the YRD during a storm event. We analyzed the morphological changes and variations in hydro-sedimentary dynamics on the tidal flat before and after the storm to assess its effects. The study aimed to answer the following queries: (1) The dynamic control mechanisms of microtidal flats in the YRD under the influence of storms and (2) the role played by storm-driven erosion in these microtidal flats.

2. Methods

2.1. Study area

The YRD, located on the western side of the Bohai Sea, is one of the river deltas with the most intense land-sea interactions globally (Yang et al., 2016). Renowned for its rich supply of fluvial sediment, the Yellow River transports a large volume of sediment from the Loess Plateau (Milliman and Meade, 1983; Wang et al., 2022). Since 1855, the Yellow River has migrated northward from the coast of the Yellow Sea to its

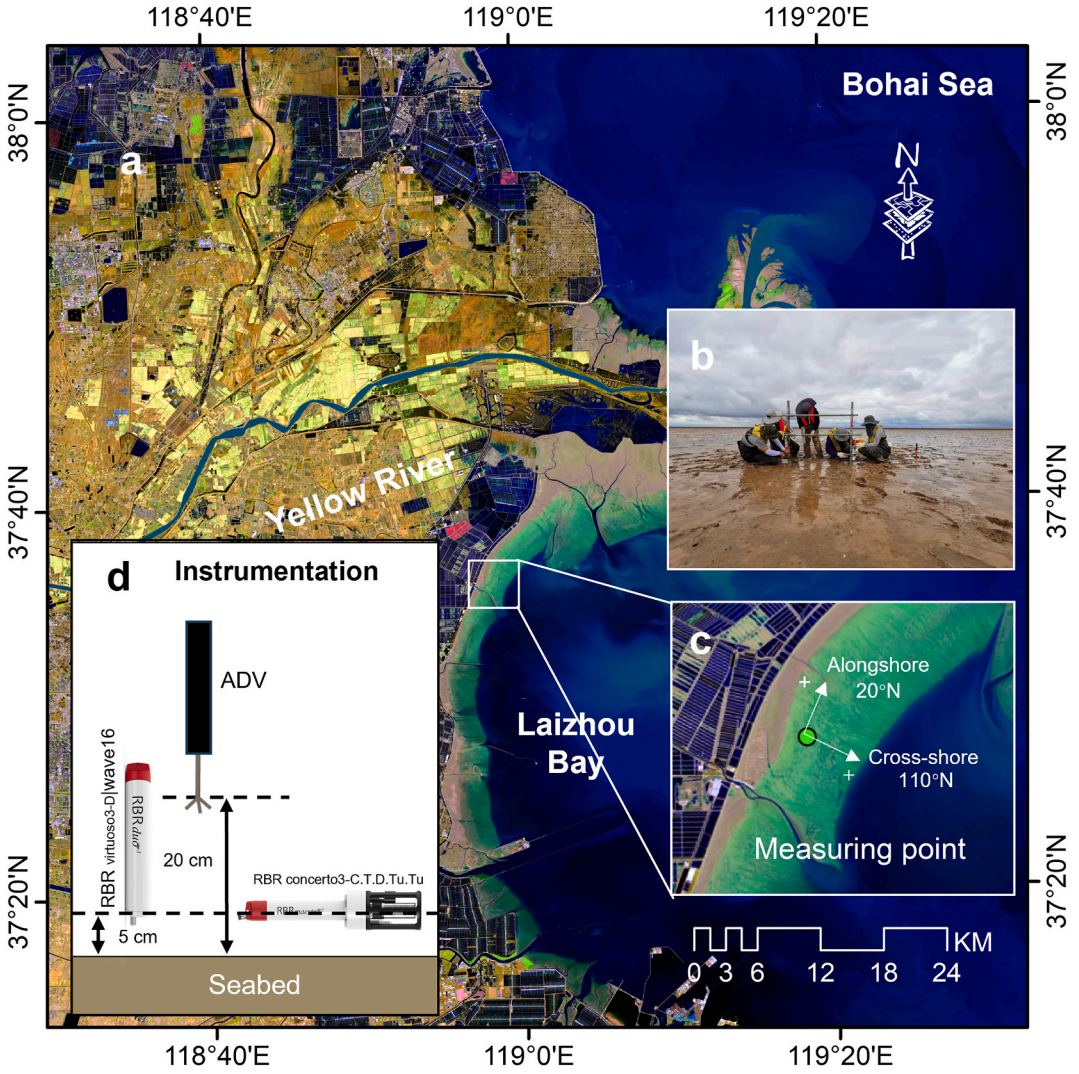

Fig. 1. (a) Map of the Yellow River Delta, (b) location of the study area and the decomposition of velocity: alongshore (20°N) and cross-shore (perpendicular to the coast,110°N), and (c) in-situ tripod at the measuring point. (For interpretation of the references to colour in this figure legend, the reader is referred to the Web version of this article.)

current outlet in the Bohai Sea (Xue, 1993). Between 1855 and 1976, the river underwent numerous changes due to sediment deposition and human activities. In 1976, human intervention redirected the course shifted from Diaokou (DK) to Qingshuigou (QSG), resulting in the present configuration of the YRD (Pang and Si, 1979). Since 1976, the DK lobe has experienced erosion, while the coastline of the QSG lobe has extended seaward, indicating accretion (Bi et al., 2021; Kuenzer et al., 2014; Wang, 2019; Zhu et al., 2021). Furthermore, in 1996, the course of the Yellow River shifted northward from Qingshuigou to the Qing8 course. The study area is situated on the southern side of the YRD and western side of Laizhou Bay (Fig. 1a). This area has experienced a continuous erosion since 1976, with an average annual shoreline retreat rate of 26.9 m/year from 1976 to 2016, although the rate of erosion has decelerated since 2000 (Chu et al., 2006; Liu et al., 2013; Zhang et al., 2018).

The tidal regime is characterized by mixed semi-diurnal tides with a microtidal range of 0.6–1.3 m. The regional wave climate is influenced by predominantly northwesterly winds in winter and southeasterly winds in summer. Extratropical storms also frequently occur and significantly influence the sediment transport and morphological changes in the YRD (Xie et al., 2021).

2.2. Field measurements

The field observation site was positioned on a mudflat approximately 100 m from the edge of salt marsh (Fig. 1b), where typical tidal flat hydrodynamic conditions were observed. The slope of the observation area was 0.8‰ (Fig. 1c). An 11-d field survey was conducted from September 28 to October 8, 2021, spanning from a neap to a spring tide period, with a storm event occurring on October 4. During this period, turbidity data were collected 5 cm above the bed using an RBR concerto^3-C.T.D.Tu., and near-bed velocities were measured with a Nortek Vector acoustic doppler velocimeter (ADV). The waves were recorded using an RBR virtuoso^3-D|wave16 via pressure sensors (Fig. 1d). The specific observational processes employed in this study are outlined in Table 1. SSC was obtained by fitting the turbidity values measured in-situ with RBR concerto^3-C.T.D.Tu. The sediment collected from adjacent to the observation site was used for calibration, revealing a linear relationship between SSC and turbidity (Fig. 2).

Surface sediments at the site were sampled before (October 3) and after (October 8) the storm (Fig. 1c). A scraper collected the sediment from a depth of 0.5 cm. After drying, 0.2 g of sediment was placed in a beaker, to which 10 mL of 10% hydrogen peroxide and hydrochloric acid were added. Following adequate reaction time, the solution was sonicated to disperse the sediment particles. Finally, sediment grain size characteristics were analyzed using a Beckman Coulter (LS13320/ULM2) laser grain size analyze, which has a range of 0.4–2000 μm and an error margin of ~2%. The proportions of clay (<4 μm), silt (4–62 μm), and sand (>62 μm) were quantified to determine their respective compositions.

Table 1
Field instruments and measurement parameters.

Instruments	Physical processes	Sampling duration/s	Sampling rate/Hz	Bursting duration/s
ADV	Currents, morphological changes	60	64	300
RBR concerto^3-C.T.D.Tu. Tu	Temperature, salinity, water depth and turbidity	30	2	300
RBR virtuoso^3-D|wave16	Waves	256	8	300

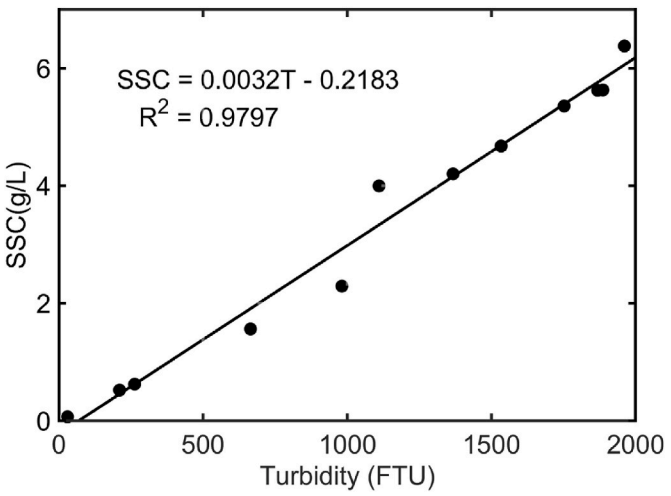

Fig. 2. Calibration of turbidity signal (FTU) with SSC.

2.3. Calculation of bed shear stress

The wave-induced bed shear stress (τ_w, N/m^2) was evaluated from the wave orbital velocity-U_δ (m/s) and the wave friction coefficient f_w (Van Rijn, 1993):

$$\tau_w = \frac{1}{2}\rho f_w U_\delta^2 \tag{1}$$

where, the peak orbital offset (A_δ) and the wave orbital velocity (U_δ) can be determined from the following equations:

$$A_\delta = \frac{H}{2\sinh(kh)} \tag{2}$$

$$U_\delta = \omega A_\delta = \frac{\pi H}{T\sinh(kh)} \tag{3}$$

where, ρ denotes the seawater density (1025kg/m^3), H indicates the wave height (m), T represents the wave period (s), h indicates the water depth (m), k represents the wave number ($k = \frac{2\pi}{L}, m^{-1}$), ω denotes the angular velocity ($\omega = \frac{2\pi}{T}, s^{-1}$), L indicates the wavelength (m) ($L = \frac{gT^2}{2\pi}\tanh(kh)$), and g indicates the gravitational acceleration ($g = 9.8m/s^{-2}$).

Wave friction coefficient f_w was calculated using the following formula (Shi et al., 2019; Soulsby, 1995):

$$f_w = 0.237r^{-0.52} \tag{4}$$

$$r = \frac{A}{k_s} \tag{5}$$

where, r and k_s denote the relative and Nikuradse grain roughness ($k_s = 2.5D_{50}, m$; D_{50} denotes the median grain size), respectively (Whitehouse et al., 2000).

The current-induced bed shear stress (τ_c, N/m^2) was evaluated using the vertical TKE method (Hu et al., 2020; Kim et al., 2000), which aims to reduce the effect of wave action on the current-induced shear stress.

$$\tau_c = c^*\rho w'^2 \tag{6}$$

where, w' denotes the vertical turbulent current velocity, and c = 0.9 indicates the proportional coefficient, which is suitable for various coastal dynamic environments (Pang et al., 2021).

The total shear stress (τ_{cw}) was evaluated by combining the wave and current process with the following formula (Soulsby, 1995):

$$\tau_{cw} = \tau_c \left[1 + 1.2\left(\frac{\tau_w}{\tau_c + \tau_w}\right)^{3.2}\right] \quad (7)$$

where, $\tau_c(N/m^2)$ and $\tau_w(N/m^2)$ represent the previously calculated shear stresses due to current and waves, respectively.

2.4. Calculation of residual currents and sediment flux

The formulas for the residual current calculation for each tidal cycle are as follows:

$$u_r = \frac{1}{T}\int_0^T u(t)dt \quad (8)$$

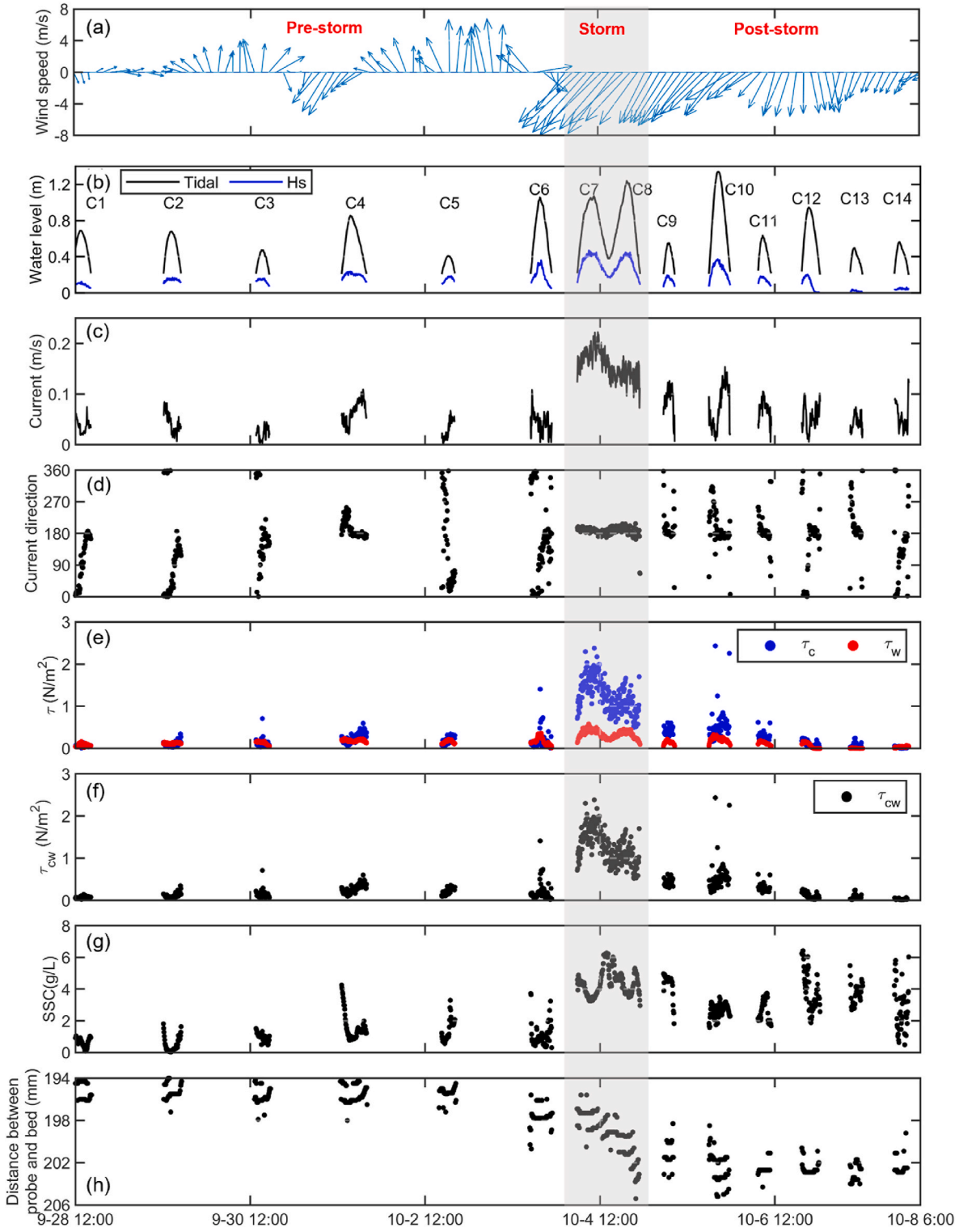

Fig. 3. Time series of (a) wind speeds, (b) tidal elevation and significant wave height (H_s), (c) current velocity, (d) current direction, (e) current-induced shear stress and wave-induced shear stress, (f) bed shear stress due to the combined current-wave action, (g) SSC, (h) changes of distance between ADV probe and bed surface.

$$v_r = \frac{1}{T}\int_0^T v(t)dt \tag{9}$$

where, u_r and v_r represent the alongshore and cross-shore components of the residual current, respectively; $u(t)$ and $v(t)$ denote the alongshore and cross-shore components of the velocity at time t, respectively; and T represents the duration of a tidal cycle.

Furthermore, the sediment flux calculation formula for each tidal cycle is:

$$Q_{si} = \frac{1}{T}\int_0^T u(t)SSC(t)dt \tag{10}$$

$$Q_{sj} = \frac{1}{T}\int_0^T v(t)SSC(t)dt \tag{11}$$

where, Q_{si} and Q_{sj} represent the alongshore and cross-shore components of sediment flux, respectively, and SSC(t) denotes the SSC at time t.

3. Results

3.1. Hydrodynamics

The study period was divided into three phases: pre-storm (C1–C6), storm (C7–C8), and post-storm (C9–C14), as depicted in Fig. 3b. Hydrodynamic conditions observed during storm events were distinct from those during fair weather. Prior to the storm (C1–C6), the study area experienced inundation once daily, despite its semi-tidal nature. Water depths did not exceed 1.0 m, and the duration of submersion was no longer than 7 h. During the storm, the elevated water levels resulted in twice daily inundations, with the maximum water level reaching 1.2 m. The tidal flat remained submerged for two tidal cycles due to storm-induced surges. Following the storm (C9–C14), the frequency of inundation continued at twice daily due to the occurrence of spring tides, although the average water depth decreased to approximately 0.5 m. The duration of inundation per tidal cycle was reduced to about 3.8 h.

3.1.1. Winds

Wind is a critical factor influencing wave development, significantly impacting wave height and direction. Wind data were sourced from the ERA5 software (https://climate.copernicus.eu/climate-reanalysis). During the storm, wind speeds ranged from 8.4 to 11.0 m/s, averaging of 10.0 m/s (Fig. 3a), and predominantly originated from the northeast (38°–50°, averaging 45°), as indicated in Fig. 4a. Under fair weather conditions, wind speeds were below 9 m/s.

3.1.2. Waves

The significant wave height (H_s) increased considerably during the

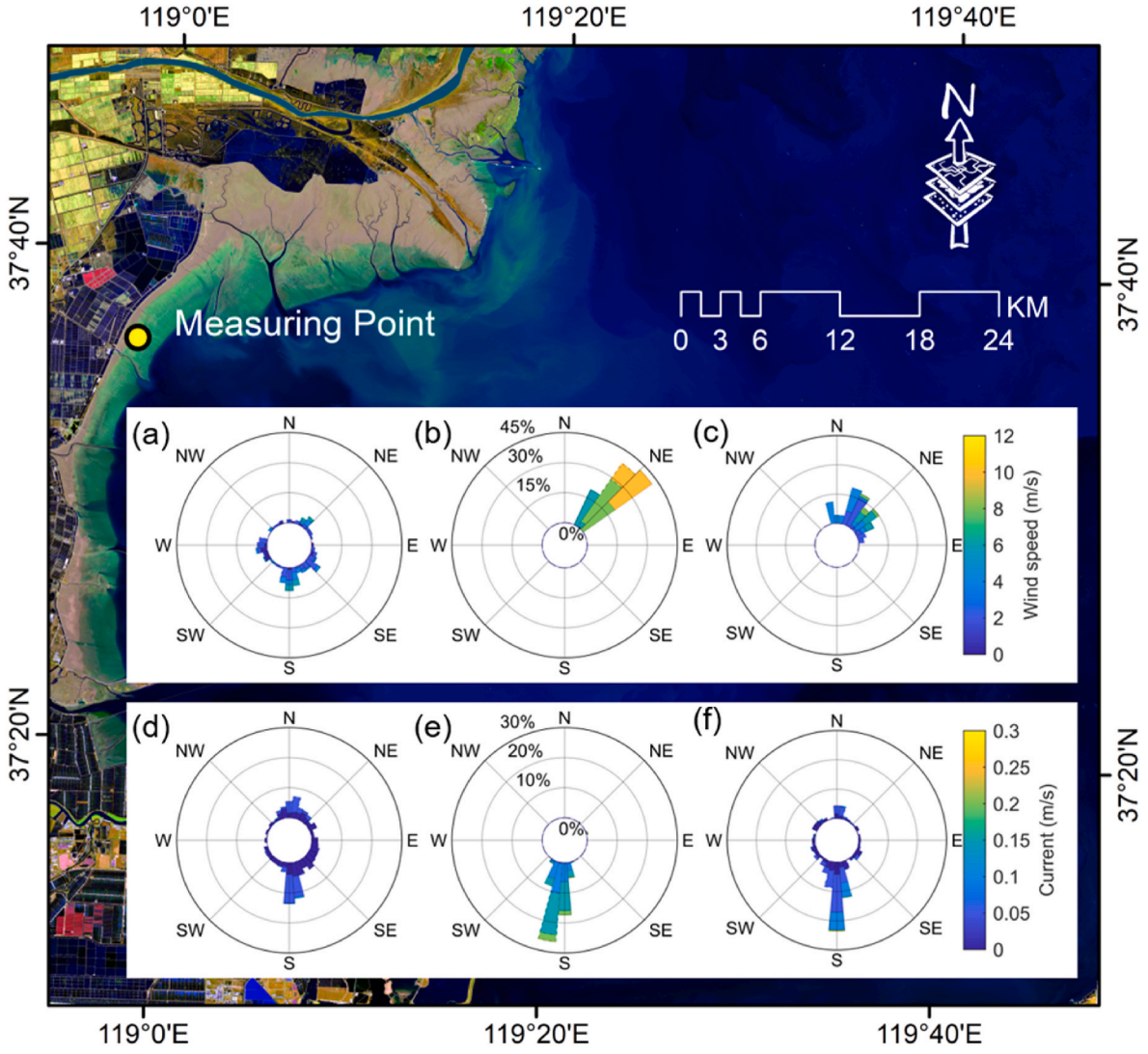

Fig. 4. Rose diagrams for wind in (a) pre-storm, (b) storm, (c) post-storm period, and current roses in (d) pre-storm, (e) storm, (f) post-storm period.

storm (Fig. 3b). The maximum H_s reached 0.47 m, with averages of 0.33 m and 0.30 m over two tidal cycles, doubling the average H_s of 0.15 m observed during the pre-storm period. After the storm, H_s swiftly returned to pre-storm levels.

3.1.3. Currents

At low water levels, the tidal flat was exposed, while at high water levels, it was completely submerged (Fig. 3b). During the pre- and post-storm phases, the average current velocity ranged from 0.02 to 0.09 m/s (Fig. 3c), increasing significantly during the storm. For instance, the average current velocity during the C7 tidal cycle was 0.18 m/s.

The storm also altered the current direction (Fig. 3d), which varied between the pre- and post-storm periods. During flood periods, the current direction shifted from 330° to 90°, and during ebb periods, it ranged from 90° to 180°, generally shifting in a clockwise direction. Throughout the storm, the tidal current consistently flowed southward at approximately 180°.

The current can be decomposed into alongshore and cross-shore directions (Fig. 1b). During the storm, the maximum average alongshore current reached 0.17 m/s (Fig. 5a), whereas the bottom offshore current was more pronounced (Fig. 5b). These significant changes in current velocity and direction may be attributed to two primary factors: wind and wind-driven waves. Earlier research demonstrated that wind speed and direction can significantly influence current velocity, thereby affecting material transport fluxes in the intertidal zone (Baeye et al., 2011; Christiansen et al., 2006). Under specific tidal and wind conditions, the current direction can reverse (Colosimo et al., 2020). Additionally, waves play a crucial role. Breaking waves create a hydraulic gradient along the coast, leading to increased current velocity. These waves transport substantial onshore momentum flux. After breaking, a certain amount of water returns offshore through bottom backflow (offshore sub-current or fissure) to maintain momentum balance within the breaking wave zone (Longuet-Higgins and Stewart, 1964). Thus, the presence of strong winds and waves during the storm potentially contributed to the observed changes in currents.

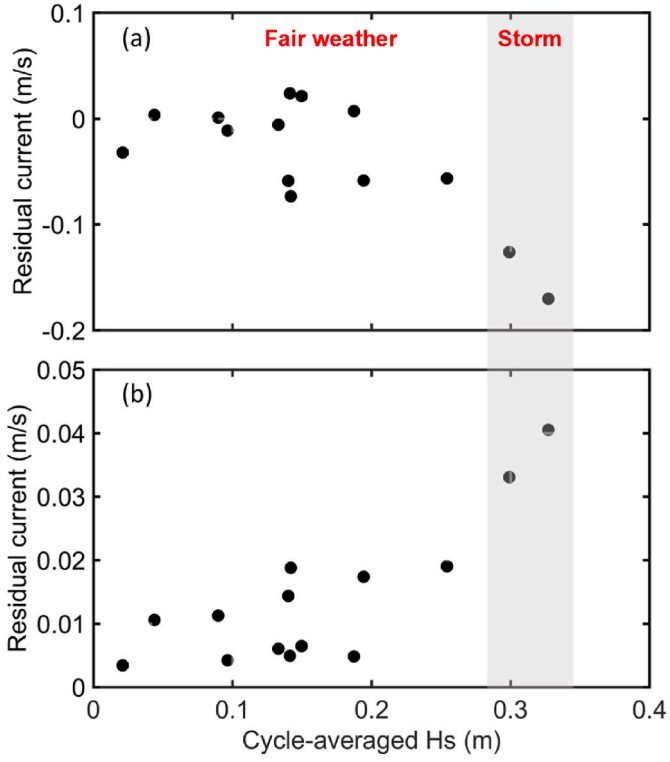

Fig. 5. Scatterplots relating averaged H_s to (a) alongshore residual current velocity, and (b) cross-shore residual current velocity within one tidal cycle, (positive values of alongshore and cross-shore currents indicates northward along the coast and offshore, respectively).

3.1.4. Bed shear stress

Bed shear stress is a critical parameter in the sediment dynamics of tidal flats, especially for calculating erosion rates (Grant and Madsen, 1979; Zhu et al., 2016). During storms, intense wave activity, different from that during fair weather conditions, cannot be overlooked. Therefore, the combined effects of waves and currents on tidal flats were considered (Shi et al., 2012; Xie et al., 2018, 2021).

During the storm, the tidal current-induced shear stress (τ_c) was 1.02–1.47 N/m^2, with an average value of 1.25 N/m^2. The wave-induced shear stress (τ_w) was 0.31–0.36 N/m^2 (Fig. 3e), and the average value was 0.33 N/m^2, which was ~25% of the tidal current-induced shear stress. The bed shear stress induced by the combined action of the current- and wave (τ_{cw}) was determined to be 1.02–1.48 N/m^2 (Fig. 3f).

In the pre-and post-storm periods, the current-induced shear stress (τ_c) varied from 0.06 to 0.60 N/m^2, with an average value of 0.22 N/m^2. The range of variations in the wave-induced shear stress was 0.04–0.21 N/m^2, and the average value was 0.12 N/m^2. The difference between the wave- and current-induced shear stresses was low. The combined shear stress (τ_{cw}) of waves and currents varied from 0.03 to 0.60 N/m^2, with an average value of 0.23 N/m^2, which was 18% of that recorded during the storm.

3.2. Sediment dynamics

3.2.1. SSC

Strong hydrodynamics during the storm led to significant sediment resuspension, resulting in an increase in SSC. Field data indicated that SSC was the highest during the storm (C7–C8) and lowest before the storm (C1–C6) (Fig. 3g). During the storm, the average SSC was 4.40 g/L, corresponding to the peak combined wave-current shear stress. Contrastingly, the pre-storm SSC ranged from 0.45 to 1.57 g/L, averaging 1.00 g/L, approximately 25% of the storm period value. In the post-storm period, SSC ranged from 2.65 to 4.11 g/L, averaging 3.30 g/L, about 75% of the storm period value. The elevated SSC post-storm suggests that the impact of storm on SSC persists, requiring a longer time for recovery to pre-storm levels.

3.2.2. Bed-level changes

The change in bed level was determined by measuring the distance between the ADV probe and the bed surface (Fig. 3h). Initially, during the pre-storm period, the bed surface was in equilibrium, with no significant changes observed throughout a tidal cycle. However, during the storm, the bed surface underwent substantial alterations, primarily exhibiting erosion. After storm C8, the cumulative erosion reached approximately 10 mm. In the subsequent post-storm period, neither significant erosion nor deposition was noted, which attributed to the diminished hydrodynamic forces and relatively low shear stress.

3.2.3. Surficial sediment grain size

During the observation period, surface sediment sampling was conducted near the observation sites. The findings revealed that the surface sediment became finer post-storm than that in the pre-storm period. Fig. 6 illustrates the sediment grain size distribution at the observation point and two adjacent locations during both periods. S1, S2, and S3 are the hydrodynamic observation point, measurement point on the mudflat, and located close to the salt marsh, respectively. Post-storm, the sediment grain size at all three locations showed a decrease, ranging from 2 to 6 μm, as detailed in Table 2. The most prominent reduction occurred at the observation site, with a decrease of ~6 μm. The sediment composition in the study area primarily consisted of silt, which constituted over 70% of the total, whereas the clay content

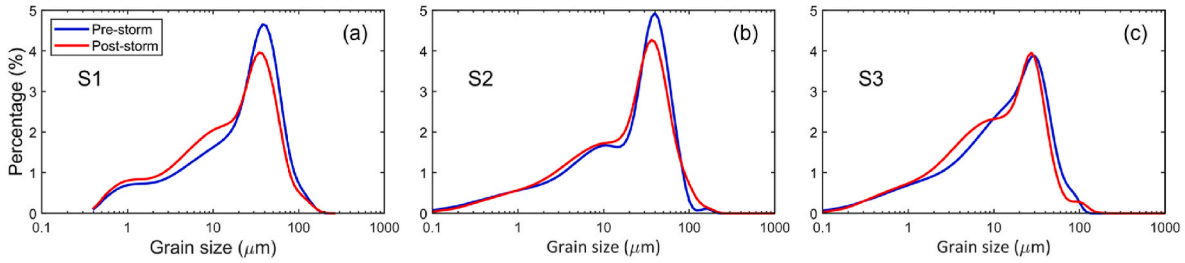

Fig. 6. Frequency distribution of sediment grain size at sampling points in pre-and post-storm period, (a) S1 at the measured point, (b) S2 near the measured point on the mudflat, and (c) S3 located closed to the marsh.

Table 2
Sediment parameters in the pre- and post-storm period.

Sampling points		Median grain size μm	Clay %	Silt %	Sand %
S1	Pre-storm	24.8	16.2	74.1	9.6
	Post-storm	18.1	19.3	73.7	6.9
S2	Pre-storm	25.1	17.6	72.4	10
	Post-storm	22.2	18.6	71.2	10.2
S3	Pre-storm	14.8	21.6	74.6	3.8
	Post-storm	12.2	24.3	73	2.8

ranged from 15% to 20%, and the sand content was the least, under 12%. A comparison of sediment components (sand, silt, and clay) between the pre- and post-storm periods revealed a slight decrease in sand content—a reduction of less than 1% in silt content—and an increase of approximately 1–3% in clay content.

4. Discussion

4.1. Controlling factors of storm-induced erosion in the YRD

The morphological evolution of tidal flats during storms is typically influenced by factors such as hydrodynamics, sediment supply, and bed surface properties (Kim et al., 2023; Mariotti et al., 2010; Priestas et al., 2015; Wang et al., 2017a). Affected by storms, coastal areas frequently experience strong winds, stormy waves, and elevated water levels (Bartholdy and Aagaard, 2001; Day et al., 2007; Kim, 2003). Given the frequent storms and the microtidal nature of the YRD, the mechanisms governing tidal flat erosion during such events need to be investigated.

Firstly, during a storm, the direct influencing factors of the erosion process are hydrodynamic conditions and sediment properties (Endler, 2009; Valentine and Mariotti, 2019). Critical shear stress, an important indicator of erosion resistance, is a key factor in this process (Leonardi et al., 2018; Shi et al., 2012; Xie et al., 2021). Liu et al. (2018) measured the critical shear stress near the study area using a cohesive sediment meter and determined that the average critical shear stress was approximately 0.8 N/m^2. It is widely recognized that erosion occurs when the combined shear stress generated by waves and currents exceeds this critical shear stress (Christiansen et al., 2006; Teisson et al., 1993). During the storm events (C7, C8) in this study, the average combined shear stress reached 1.48 and 1.02 N/m^2, respectively, surpassing the critical stress and resulting in significant erosion of the bed surface (~10 mm) and substantial sediment resuspension. The average SSC during the storm was 4.40 g/L, which was significantly higher than that of the pre-storm average of 1.00 g/L (Fig. 3g). This type of erosion caused by storms was also observed on other tidal flats (de Vet et al., 2020; Xie et al., 2017; Yang et al., 2003). When the storm intensity is weaker, the shear stress does not exceed the critical shear stress of the tidal flat, which is insufficient to cause erosion (Xie et al., 2021). Therefore, storm intensity plays a significant role in the bed changes of tidal flats. In this study, considering the maximum wind speed and duration, we identified and counted the number of storms with intensity comparable to or exceeding that of this storm, averaging six occurrences per year, indicating that the intensity of this storm was among the severe storms. Therefore, the high shear stress generated by intense storms leads to direct erosion.

Secondly, sediment transport during storms can significantly alter the morphology through cross-shore and alongshore transport. Storms can cause extensive erosion or deposition on tidal flats, largely because of the strong hydrodynamic forces they generate, with sediment transport being another significant factor (Bartholdy and Aagaard, 2001; Colosimo et al., 2020; Day et al., 2007). When sediments are transported toward the shore, they can supply a substantial amount of sediment to tidal flats, leading to deposition (Siadatmousavi and Jose, 2015; Tognin et al., 2021; Turner et al., 2006; Xie et al., 2021). In regions, such as the US Gulf Coast and the Mediterranean, wind-driven storm surges play a crucial role in delivering sediments to salt marshes, with sediment contributions from major storms could be equating to several years of sedimentation under non-storm conditions (Dietz et al., 2018; McKee and Cherry, 2009). For erosion induced by storms, sediment tends to be transported toward salt marshes or nearby offshore areas (Yang et al., 2003). In the study area, the storm altered the direction of currents, leading to southward and offshore sediment transport (Fig. 7). The sediment flux of alongshore transport was approximately four times that of cross-shore transport, indicating that storm-induced erosion made the resuspended sediment a source of alongshore sediment transport.

Furthermore, the bed sediment characteristics significantly influence erosion processes, as evidenced by multiple studies (Liu et al., 2018; Meng et al., 2012; Valentine and Mariotti, 2019). Research reported that sediments in erosion zones post-typhoon is typically coarser than that in fair weather conditions (Fan et al., 2006). Contrarily, this study found that the surficial sediment in post-storm periods became finer than that in pre-storm periods, with the median grain size decreasing by approximately 10–25% (Fig. 6). This discrepancy may emerge from the differences in study areas; Fan et al. (2006) focused on an accretional tidal flat, where sediment deposition was relatively loose, leading to the predominance of coarser sediments due to the erosion of finer grains during storms. In erosional tidal flats, the critical bed shear stress is relatively high, indicating that greater shear stress is required to initiate erosion (Xie et al., 2021, 2023). During the storm analyzed in this study, the combined wave-current shear stress did not consistently exceed the critical shear stress. Specifically, during the storm C7 and C8, the combined wave-current shear stress was below the critical shear stress at the beginning and end of these tidal cycles (Fig. 3f), preventing ongoing erosion. This condition potentially facilitated an exchange between the suspended and bed sediments toward the end of C8. The high SSC observed during the storm originated from two primary sources: the resuspension of bed sediment due to high shear stress and the influx of sediment from surrounding areas into the study zone, which increased the SSC. Earlier studies demonstrated that under the influence of northerly winds, sediment transport in this region predominantly moves

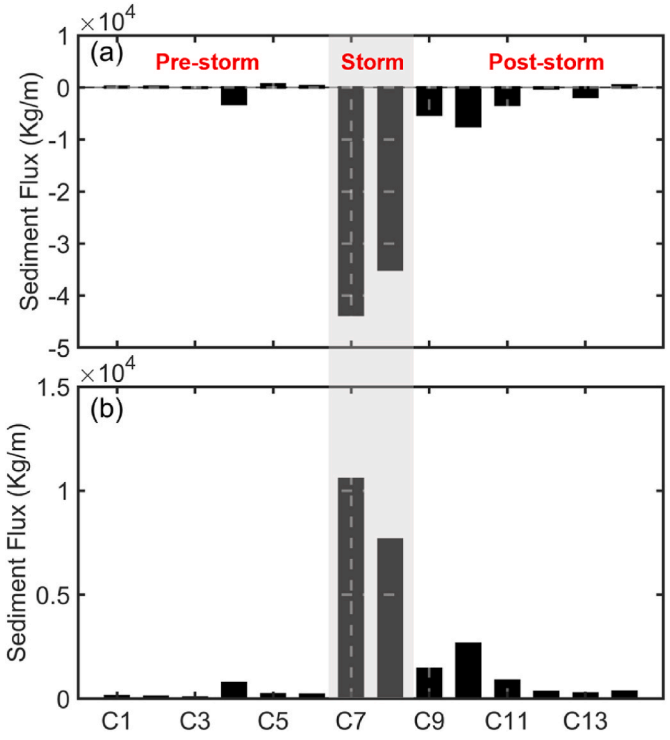

Fig. 7. (a) Alongshore and (b) cross-shore net sediment flux, the positive value of alongshore transport represents northward, and the positive value of cross-shore transport implies offshore.

southward along the coast, reaching the central part of Laizhou Bay (Fan et al., 2020; Fu et al., 2021; Li et al., 2022; Yao et al., 2020). The present observations align with those of these findings, showing a significant southward sediment transport during the storm (Fig. 7). At the end of the storm, it is hypothesized that suspended sediment was replaced by fine-grained sediment from adjacent areas. This hypothesis is supported by the maintained high SSC post-storm. The SSC after the storm (about 3.5 g/L, Fig. 8) exceeded the pre-stormlevels, suggesting that currents transported more sediment from adjacent waters to the tidal flat during the post-storm period. The hydrodynamic conditions were weaker during the C12–C14 period (Fig. 8), allowing only fine sediments to be transported to the study area by tidal currents (Winterwerp et al., 2012). Fine sediments are easily eroded and transported by currents and waves.

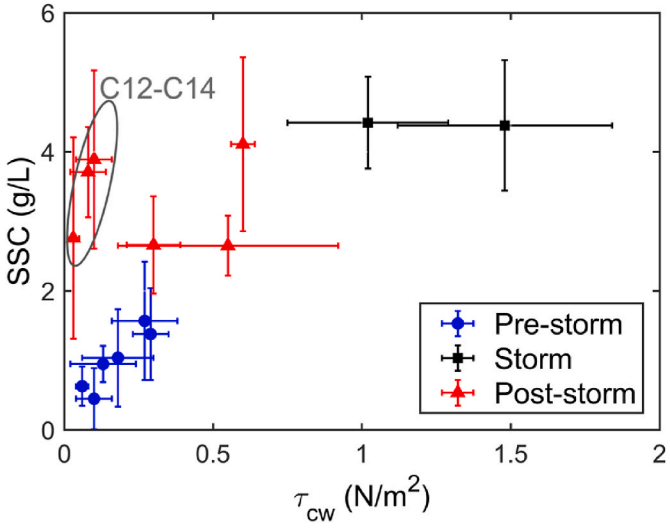

Fig. 8. Scatterplots relating bed shear stress to SSC.

The grain size and composition of sediment are closely associated with the critical shear stress, which influences the erosion and deposition processes on tidal flats (Meng et al., 2012). These factors are crucial in the entrainment, transport, deposition, and compaction of sediment particles, playing a critical role in the evolution of tidal flats (Liu et al., 2022).

Conclusively, during this intense storm, high shear stress and changes of sediment transport led to the direct erosion of the tidal flat. Additionally, the impact of the storm on bed sediment may influence the subsequent tidal flat evolution, which warrants further research.

4.2. *Role of the storm in the erosional microtidal flat*

During storms, increased wave energy and current velocity contribute to significant erosion, which is observable within a short timeframe on tidal flats (de Vet et al., 2020; Xie et al., 2021; Yang et al., 2003). Such conditions can expedite coastal erosion rates on erosional coasts exemplified by the Mississippi Delta (Dietz et al., 2018; Rangoonwala et al., 2016). In this study, storms were identified as the primary factor influencing the evolution of microtidal flats in the YRD.

Under fair weather conditions, on mesotidal or macrotidal flats, such as those in the Eastern Chongming Wetland of the Yangtze Estuary, elevation changes of up to 5 cm can occur within a single tidal cycle, accumulating to approximately 10 cm over a 10-d period (Shi et al., 2017). Research indicates that for microtidal flats in equilibrium between erosion and deposition, the bed level may alter by less than 1.5 cm within a tidal cycle (Christiansen et al., 2006). For the erosional microtidal flat in the southern YRD, earlier studies documented ongoing erosion since the 1970s, with the coastline retreating at a rate of tens of meters annually (Fu et al., 2021; Wang, 2019). Specifically, the study area experienced erosion between 1996 and 2016, and accretion from 1976 to 1996. In 1976, human intervention redirected the course of the Yellow River from Diaokou (DK) to Qingshuigou (QSG), resulting in the current configuration of the YRD (Pang and Si, 1979). The sediment carried by the Yellow River was transported to the southern YRD, potentially resulting in the accretion observed between 1976 and 1996. In 1996, the course of the Yellow River shifted northward, moving from Qingshuigou to the Qing8 course. This course change significantly extended the sediment transport path to the study area. Additionally, human activities upstream considerably reduced the sediment discharge of the Yellow River (Ji et al., 2020). The decrease in sediment discharge and the course change possibly contributed to the erosion observed in the area after 1996. However, the southern tidal flats of the YRD, compared to those of the current estuary and northern parts, have remained relatively stable, with smaller shoreline changes (Xu et al., 2019). The shoreline in the study area experienced significant retreat from 1996 to 2003, although the retreat rate decreased after 2003 (Zhu et al., 2021; Fu et al., 2021). The present findings indicate that during fair weather, the bed level exhibited minor fluctuations within a range of ±2 mm (Fig. 3h). Additionally, the combined bed shear stress of waves and currents measured on-site (Fig. 8) was significantly below the critical shear stress, indicating that significant changes to the tidal flat were unlikely. Contrastingly, during the storm (C7 and C8), the tidal flat remained submerged due to the storm surge occurring during medium-tide periods. Nonetheless, the water levels were comparable to those during spring tides (Fig. 3b). The average combined bed shear stress during these conditions significantly exceeded the critical shear stress, resulting in substantial bed erosion (~10 mm, Fig. 3h). Therefore, only extreme storm events are capable of disrupting the equilibrium maintained under fair weather conditions, leading to erosion of the microtidal flat.

Additionally, it is crucial to acknowledge that in the YRD, the post-storm recovery process was inadequate to counterbalance the erosion caused by storms. Sediment supply is the dominant factor affecting tidal flats. When sediment supply is ample, accretion occurs, and erosion occurs when sediment supply is insufficient (Gao, 2019; Mariotti and

Fagherazzi, 2010). Storms can temporarily disrupt the balance, between erosion and deposition, leading to short-term imbalances (Choi et al., 2023; Christiansen et al., 2006; Zhou et al., 2022). Tidal flats with abundant sediment supply rapidly recover from storm-induced erosion (Xie et al., 2017; Yang et al., 2003), while those lacking sediment always experience erosion without recovery (Gao, 2019; Zhu and Wiberg, 2022). Due to the limited submersion period and weak hydrodynamic forces in microtidal flats during fair weather conditions (Day et al., 2007; McKee and Cherry, 2009; Yang et al., 2003), the morphological recovery time following a storm is significantly longer than that of mesotidal and macrotidal flats. The YRD is frequently impacted by extratropical storms and cold fronts (Fan et al., 2020; Fu et al., 2021), which contribute to ongoing erosion of tidal flats (Leonardi et al., 2016; Valentine and Mariotti, 2019). Consequently, tidal flats may not recuperate from storm-induced erosion, resulting in continuous shoreline retreat.

Our study found that under conditions of limited sediment supply, the tidal flat morphology approached a state of equilibrium during fair weather conditions, showing neither significant erosion nor accretion. However, individual storms caused erosion that was difficult to recover from, suggesting that cumulative erosion from multiple storms throughout the year is a key factor in shoreline retreat. However, this study has limitations that are addressed before concluding. The field observation period spanned 11 d, focusing on hydrodynamic and sediment characteristics during the spring-neap cycle. However, the hydrodynamic and sedimentary processes of the Yellow River also display pronounced seasonal variations (Wang et al., 2017b; Wu et al., 2015), and the impacts of summer and winter storms differ significantly (Jin et al., 2023; Niu et al., 2023; Yang et al., 2011). Therefore, to accurately comprehend the mechanisms of hydrodynamics, sediment transport, and morphological evolution in this region, long-term monitoring is essential to capture seasonal variations and different storm types. Furthermore, the reduction in sediment supply from the Yellow River may also be a contributing factor (Fu et al., 2021; Zhang et al., 2018; Zhu et al., 2021). However, assessing the relative importance and contributions of these factors necessitates long-term data and further research.

5. Conclusions

An 11-d field survey was conducted on the southern tidal flat of the YRD to investigate the erosion mechanisms induced by storms in a microtidal flat. During fair weather, the study area experienced shorter inundation periods and weaker hydrodynamics. The combined bed shear stress of waves and currents, measured on-site at 0.03–0.60 N/ m^2, was significantly below the critical shear stress. Additionally, minimal bed level fluctuations (within ±2 mm) were observed, indicating that the tidal flat had reached an equilibrium state.

However, the storm disrupted the equilibrium state maintained under fair weather conditions. The hydrodynamic changes induced by the storm were mainly reflected in increased current velocity and significant wave height, with the current consistently flowing southward at approximately 180°. This resulted in high shear stresses (ranging from 1.02 to 1.48 N/m^2) and significant alongshore sediment transport, causing erosion of 10 mm. Additionally, the storm altered properties of the bed sediment, with the median diameter decreasing by 2–6 μm.

Post-storm recovery was insubstantial. Due to short submerged periods and weak hydrodynamics, the morphological recovery time following a storm is significantly longer than that of the mesotidal and macrotidal flats. This prolonged recovery time hinders the ability to quickly counteract storm-induced erosion. Therefore, frequent storms pose a risk of perpetuating continuous shoreline retreat along the microtidal coast.

CRediT authorship contribution statement

Haisheng Yu: Writing – review & editing, Writing – original draft, Visualization, Software, Resources, Methodology, Investigation, Formal analysis, Data curation, Conceptualization. **Weiming Xie:** Writing – review & editing, Writing – original draft, Validation, Software, Resources, Methodology, Investigation, Funding acquisition, Formal analysis, Data curation, Conceptualization. **Zhong Peng:** Writing – review & editing, Supervision, Resources, Methodology, Investigation, Funding acquisition, Formal analysis, Data curation, Conceptualization. **Fan Xu:** Writing – review & editing, Validation, Supervision, Methodology, Data curation, Conceptualization. **Jianwei Sun:** Writing – review & editing, Visualization, Validation, Formal analysis, Conceptualization. **Qing He:** Writing – review & editing, Validation, Methodology, Funding acquisition, Formal analysis, Data curation, Conceptualization.

Declaration of competing interest

The authors declare that they have no known competing financial interests or personal relationships that could have appeared to influence the work reported in this paper.

Data availability

Data will be made available on request.

Acknowledgments

This work is financially supported by the National Natural Science Foundation of China (Nos. U2040216, 42476215, U2243207, 42276217, 51909101). Financial support from the National Key Research and Development Program of China (2022YFE0136700) is also acknowledged. This paper is also funded by the project of Key Laboratory of Changjiang Regulation and Protection of Ministry of Water Resources, China (CX 2023K05). The authors thank Prof. Zheng Bing Wang, Prof. Bas van Maren and Prof. Huib de Vriend for their insightful discussions. The authors thank Zhonghao Zhao, Yufan Chen, Tianyou Li, Ying Zhao, Zhiyang Zhu and Ke Deng for their assistance with the field observations. Finally, we express our gratitude to the reviewers and editors for their valuable comments and suggestions, which greatly contributed to improving the quality of this paper.

References

Bacmeister, J.T., Reed, K.A., Hannay, C., Lawrence, P., Bates, S., Truesdale, J.E., Rosenbloom, N., Levy, M., 2018. Projected changes in tropical cyclone activity under future warming scenarios using a high-resolution climate model. Climatic Change 146 (3), 547–560. https://doi.org/10.1007/s10584-016-1750-x.

Baeye, M., Fettweis, M., Voulgaris, G., Van Lancker, V., 2011. Sediment mobility in response to tidal and wind-driven flows along the Belgian inner shelf, southern North Sea. Ocean Dynam. 61 (5), 611–622. https://doi.org/10.1007/s10236-010-0370-7.

Bartholdy, J., Aagaard, T., 2001. Storm surge effects on a back-barrier tidal flat of the Danish Wadden Sea. Geo Mar. Lett. 20 (3), 133–141. https://doi.org/10.1007/s003670000048.

Bi, N., Wang, H., Wu, X., Saito, Y., Xu, C., Yang, Z., 2021. Phase change in evolution of the modern huanghe (Yellow River) delta: process, pattern, and mechanisms. Mar. Geol. 437, 106516. https://doi.org/10.1016/j.margeo.2021.106516.

Choi, S.M., Seo, J.Y., Ha, H.K., 2023. Contribution of local erosion enhanced by winds to sediment transport in intertidal flat. Mar. Geol. 465, 107171. https://doi.org/10.1016/j.margeo.2023.107171.

Christiansen, C., Vølund, G., Lund-Hansen, L.C., Bartholdy, J., 2006. Wind influence on tidal flat sediment dynamics: field investigations in the Ho Bugt, Danish Wadden Sea. Mar. Geol. 235 (1), 75–86. https://doi.org/10.1016/j.margeo.2006.10.006.

Christie, M.C., Dyer, K.R., Turner, P., 2000. Observations of long and short term variations in the bed elevation of a macro-tidal mudflat. In: McAnally, W.H., Mehta, A.J. (Eds.), Proceedings in Marine Science, vol. 3. Elsevier, pp. 323–342. https://doi.org/10.1016/S1568-2692(00)80129-1.

Chu, Z.X., Sun, X.G., Zhai, S.K., Xu, K.H., 2006. Changing pattern of accretion/erosion of the modern Yellow River (Huanghe) subaerial delta, China: based on remote sensing images. Mar. Geol. 227 (1), 13–30. https://doi.org/10.1016/j.margeo.2005.11.013.

Colosimo, I., de Vet, P.L.M., van Maren, D.S., Reniers, A.J.H.M., Winterwerp, J.C., van Prooijen, B.C., 2020. The impact of wind on flow and sediment transport over intertidal flats. J. Mar. Sci. Eng. 8 (11).

Day, J.W., Boesch, D.F., Clairain, E.J., Kemp, G.P., Laska, S.B., Mitsch, W.J., Orth, K., Mashriqui, H., Reed, D.J., Shabman, L., Simenstad, C.A., Streever, B.J., Twilley, R.R., Watson, C.C., Wells, J.T., Whigham, D.F., 2007. Restoration of the Mississippi delta:

lessons from hurricanes katrina and rita. Science 315 (5819), 1679–1684. https://doi.org/10.1126/science.1137030.
de Vet, P.L.M., van Prooijen, B.C., Colosimo, I., Steiner, N., Ysebaert, T., Herman, P.M.J., Wang, Z.B., 2020. Variations in storm-induced bed level dynamics across intertidal flats. Sci. Rep. 10 (1), 12877. https://doi.org/10.1038/s41598-020-69444-7.
Dietz, M.E., Liu, K.-b., Bianchette, T.A., 2018. Hurricanes as a major driver of coastal erosion in the Mississippi River Delta: a multi-decadal analysis of shoreline retreat rates at Bay champagne, Louisiana (USA). Water 10 (10), 1480. https://www.mdpi.com/2073-4441/10/10/1480.
Endler, R., 2009. Sediment physical properties of the DYNAS study area. J. Mar. Syst. 75 (3), 317–329. https://doi.org/10.1016/j.jmarsys.2007.09.012.
Fan, D., Guo, Y., Wang, P., Shi, J.Z., 2006. Cross-shore variations in morphodynamic processes of an open-coast mudflat in the Changjiang Delta, China: with an emphasis on storm impacts. Continent. Shelf Res. 26 (4), 517–538. https://doi.org/10.1016/j.csr.2005.12.011.
Fan, Y., Chen, S., Pan, S., Dou, S., 2020. Storm-induced hydrodynamic changes and seabed erosion in the littoral area of Yellow River Delta: a model-guided mechanism study. Continent. Shelf Res. 205, 104171. https://doi.org/10.1016/j.csr.2020.104171.
Fu, Y., Chen, S., Ji, H., Fan, Y., Li, P., 2021. The modern Yellow River Delta in transition: causes and implications. Mar. Geol. 436, 106476. https://doi.org/10.1016/j.margeo.2021.106476.
Gao, S., 2019. Chapter 10 - geomorphology and sedimentology of tidal flats. In: Perillo, G.M.E., Wolanski, E., Cahoon, D.R., Hopkinson, C.S. (Eds.), Coastal Wetlands, second ed. Elsevier, pp. 359–381. https://doi.org/10.1016/B978-0-444-63893-9.00010-1.
Grant, W.D., Madsen, O.S., 1979. Combined wave and current interaction with a rough bottom. J. Geophys. Res.: Oceans 84 (C4), 1797–1808. https://doi.org/10.1029/JC084iC04p01797.
Hu, B.P., Xie, J., Li, W., He, Z., Marsooli, R., Wu, W., 2020. A RANS numerical study of experimental swash flows and its bed shear stress estimation. Appl. Ocean Res. 100, 102145. https://doi.org/10.1016/j.apor.2020.102145.
Isla, M.F., Guisado-Pintado, E., Rodríguez-Galiano, V.F., López-Nieta, D., 2024. Effects of major storms over a spit-tidal flat interaction system (Punta Rasa-Samborombón, Argentina). Sci. Total Environ. 930, 172818. https://doi.org/10.1016/j.scitotenv.2024.172818.
Jin, S., Fagherazzi, S., Fichot, C.G., Wu, X., Liu, Y.X., Zheng, X., Zou, T., Xing, Q., 2023. Drivers of suspended sediment dynamics along the shorelines of the Yellow River Delta detected from satellite data. Earth Surf. Process. Landforms 48 (15), 3091–3102. https://doi.org/10.1002/esp.5683.
Kim, B.O., 2003. Tidal modulation of storm waves on a macrotidal flat in the Yellow Sea. Estuar. Coast Shelf Sci. 57 (3), 411–420. https://doi.org/10.1016/S0272-7714(02)00369-4.
Kim, K.-H., Kim, M.-S., Lee, H.M., Kim, M.H., Woo, S.-B., 2023. Dominant factors responsible for wave modulation in the macro-tidal Gyeonggi Bay of the Yellow Sea. Ocean Eng. 287, 114875. https://doi.org/10.1016/j.oceaneng.2023.114875.
Kim, S.C., Friedrichs, C.T., Maa, J.P.Y., Wright, L.D., 2000. Estimating bottom stress in tidal boundary layer from acoustic Doppler velocimeter data. J. Hydraul. Eng. 126 (6), 399–406. https://doi.org/10.1061/(ASCE)0733-9429(2000)126:6(399.
Kirwan, M.L., Megonigal, J.P., 2013. Tidal wetland stability in the face of human impacts and sea-level rise. Nature 504 (7478), 53–60. https://doi.org/10.1038/nature12856.
Kuenzer, C., Ottinger, M., Liu, G., Sun, B., Baumhauer, R., Dech, S., 2014. Earth observation-based coastal zone monitoring of the Yellow River Delta: dynamics in China's second largest oil producing region over four decades. Appl. Geogr. 55, 92–107. https://doi.org/10.1016/j.apgeog.2014.08.015.
Leonardi, N., Carnacina, I., Donatelli, C., Ganju, N.K., Plater, A.J., Schuerch, M., Temmerman, S., 2018. Dynamic interactions between coastal storms and salt marshes: a review. Geomorphology 301, 92–107. https://doi.org/10.1016/j.geomorph.2017.11.001.
Leonardi, N., Ganju, N.K., Fagherazzi, S., 2016. A linear relationship between wave power and erosion determines salt-marsh resilience to violent storms and hurricanes. Proc. Natl. Acad. Sci. USA 113 (1), 64–68. https://doi.org/10.1073/pnas.1510095112.
Li, B., Liu, J.P., Jia, Y., 2022. Comparison of the causes of erosion–deposition between Yellow River, Yangtze river, and mekong river subaqueous delta l: model building. Water 14 (20).
Liu, L., Wang, H., Yang, Z., Fan, Y., Wu, X., Hu, L., Bi, N., 2022. Coarsening of sediments from the Huanghe (Yellow River) delta-coast and its environmental implications. Geomorphology 401, 108105. https://doi.org/10.1016/j.geomorph.2021.108105.
Liu, X.-L., Zheng, J.-W., Zhang, H., Zhang, S.-T., Liu, B.-H., Shan, H.-X., Jia, Y.-G., 2018. Sediment critical shear stress and geotechnical properties along the modern Yellow River Delta, China. Mar. Georesour. Geotechnol. 36 (8), 875–882. https://doi.org/10.1080/1064119X.2017.1393477.
Liu, Y., Huang, H., Qiu, Z., Fan, J., 2013. Detecting coastline change from satellite images based on beach slope estimation in a tidal flat. Int. J. Appl. Earth Obs. Geoinf. 23, 165–176. https://doi.org/10.1016/j.jag.2012.12.005.
Longuet-Higgins, M.S., Stewart, R.w., 1964. Radiation stresses in water waves; a physical discussion, with applications. Deep Sea Research and Oceanographic Abstracts. 11 (4), 529–562. https://doi.org/10.1016/0011-7471(64)90001-4.
Mariotti, G., Fagherazzi, S., 2010. A numerical model for the coupled long-term evolution of salt marshes and tidal flats. J. Geophys. Res.: Earth Surf. 115 (F1). https://doi.org/10.1029/2009JF001326.
Mariotti, G., Fagherazzi, S., Wiberg, P.L., McGlathery, K.J., Carniello, L., Defina, A., 2010. Influence of storm surges and sea level on shallow tidal basin erosive processes. J. Geophys. Res.: Oceans 115 (C11). https://doi.org/10.1029/2009JC005892.
McKee, K.L., Cherry, J.A., 2009. Hurricane Katrina sediment slowed elevation loss in subsiding brackish marshes of the Mississippi River delta. Wetlands 29 (1), 2–15. https://doi.org/10.1672/08-32.1.
Meng, X.-m., Jia, Y.-g., Shan, H.-x., Yang, Z.-n., Zheng, J.-w., 2012. An experimental study on erodibility of intertidal sediments in the Yellow River delta. Int. J. Sediment Res. 27 (2), 240–249. https://doi.org/10.1016/S1001-6279(12)60032-8.
Milliman, J.D., Meade, R.H., 1983. World-wide delivery of river sediment to the oceans. J. Geol. 91 (1), 1–21. http://www.jstor.org/stable/30060512.
Niu, J., Xie, J., Lin, S., Lin, P., Gao, F., Zhang, J., Cai, S., 2023. Importance of bed liquefaction-induced erosion during the winter wind storm in the Yellow River Delta, China. J. Geophys. Res.: Oceans 128 (10), e2022JC019256. https://doi.org/10.1029/2022JC019256.
Pang, J., Si, S., 1979. The estuary changes of Huanghe River I. Changes in modern time. Oceanol. Limnol. Sinica 10 (2), 136–142.
Pang, W., Zhou, X., Dai, Z., Li, S., Huang, H., Lei, Y., 2021. ADV-based investigation on bed level changes over a meso-macro tidal beach. Front. Mar. Sci. 8. https://doi.org/10.3389/fmars.2021.733923.
Pannozzo, N., Leonardi, N., Carnacina, I., Smedley, R.K., 2023. Storm sediment contribution to salt marsh accretion and expansion. Geomorphology 430, 108670. https://doi.org/10.1016/j.geomorph.2023.108670.
Priestas, A.M., Mariotti, G., Leonardi, N., Fagherazzi, S., 2015. Coupled wave energy and erosion dynamics along a salt marsh boundary, hog island Bay, Virginia, USA. J. Mar. Sci. Eng. 3 (3), 1041–1065.
Rangoonwala, A., Jones, C.E., Ramsey Iii, E., 2016. Wetland shoreline recession in the Mississippi River Delta from petroleum oiling and cyclonic storms. Geophys. Res. Lett. 43 (22), 660. https://doi.org/10.1002/2016GL070624, 11,652-611.
Shi, B., Cooper, J.R., Li, J., Yang, Y., Yang, S.L., Luo, F., Yu, Z., Wang, Y.P., 2019. Hydrodynamics, erosion and accretion of intertidal mudflats in extremely shallow waters. J. Hydrol. 573, 31–39. https://doi.org/10.1016/j.jhydrol.2019.03.065.
Shi, B.W., Yang, S.L., Wang, Y.P., Bouma, T.J., Zhu, Q., 2012. Relating accretion and erosion at an exposed tidal wetland to the bottom shear stress of combined current–wave action. Geomorphology 138 (1), 380–389. https://doi.org/10.1016/j.geomorph.2011.10.004.
Shi, B.W., Yang, S.L., Wang, Y.P., Li, G.C., Li, M.L., Li, P., Li, C., 2017. Role of wind in erosion-accretion cycles on an estuarine mudflat. J. Geophys. Res.: Oceans 122 (1), 193–206. https://doi.org/10.1002/2016JC011902.
Siadatmousavi, S.M., Jose, F., 2015. Winter storm-induced hydrodynamics and morphological response of a shallow transgressive shoal complex: northern Gulf of Mexico. Estuar. Coast Shelf Sci. 154, 58–68. https://doi.org/10.1016/j.ecss.2014.12.025.
Soulsby, R., 1995. Bed shear-stresses due to combined waves and currents. Advances in coastal morphodynamics.
Spiske, M., Pilarczyk, J.E., Mitchell, S., Halley, R.B., Otai, T., 2022. Coastal erosion and sediment reworking caused by hurricane Irma – implications for storm impact on low-lying tropical islands. Earth Surf. Process. Landforms 47 (4), 891–907. https://doi.org/10.1002/esp.5293.
Teisson, C., Ockenden, M., Le Hir, P., Kranenburg, C., Hamm, L., 1993. Cohesive sediment transport processes. Coastal Engineering. 21 (1), 129–162. https://doi.org/10.1016/0378-3839(93)90048-D.
Tognin, D., D'Alpaos, A., Marani, M., Carniello, L., 2021. Marsh resilience to sea-level rise reduced by storm-surge barriers in the Venice Lagoon. Nat. Geosci. 14 (12), 906–911. https://doi.org/10.1038/s41561-021-00853-7.
Turner, R.E., Baustian, J.J., Swenson, E.M., Spicer, J.S., 2006. Wetland sedimentation from hurricanes katrina and rita. Science 314 (5798), 449–452. https://doi.org/10.1126/science.1129116.
Valentine, K., Mariotti, G., 2019. Wind-driven water level fluctuations drive marsh edge erosion variability in microtidal coastal bays. Continent. Shelf Res. 176, 76–89. https://doi.org/10.1016/j.csr.2019.03.002.
van der Wegen, M., Jaffe, B., Foxgrover, A., Roelvink, D., 2017. Mudflat morphodynamics and the impact of sea level rise in south San Francisco Bay. Estuar. Coast 40 (1), 37–49. https://doi.org/10.1007/s12237-016-0129-6.
Van Rijn, L.C., 1993. Principles of Sediment Transport in Rivers, Estuaries and Coastal Seas, vol. 1006. Aqua publications, Amsterdam.
Wang, H., van der Wal, D., Li, X., van Belzen, J., Herman, P.M.J., Hu, Z., Ge, Z., Zhang, L., Bouma, T.J., 2017a. Zooming in and out: scale dependence of extrinsic and intrinsic factors affecting salt marsh erosion. J. Geophys. Res.: Earth Surf. 122 (7), 1455–1470. https://doi.org/10.1002/2016JF004193.
Wang, H., Wu, X., Bi, N., Li, S., Yuan, P., Wang, A., Syvitski, J.P.M., Saito, Y., Yang, Z., Liu, S., Nittrouer, J., 2017b. Impacts of the dam-orientated water-sediment regulation scheme on the lower reaches and delta of the Yellow River (Huanghe): a review. Global Planet. Change 157, 93–113. https://doi.org/10.1016/j.gloplacha.2017.08.005.
Wang, J., Shi, B., Zhao, E., Yuan, Q., Chen, X., 2022. The long-term spatial and temporal variations of sediment loads and their causes of the Yellow River Basin. Catena 209, 105850. https://doi.org/10.1016/j.catena.2021.105850.
Wang, K., 2019. Evolution of Yellow River Delta coastline based on remote sensing from 1976 to 2014, China. Chin. Geogr. Sci. 29 (2), 181–191. https://doi.org/10.1007/s11769-019-1023-5.
Whitehouse, R., Soulsby, R., Roberts, W., Mitchener, H., 2000. Dynamics of Estuarine Muds.
Winterwerp, J.C., van Kesteren, W.G.M., van Prooijen, B., Jacobs, W., 2012. A conceptual framework for shear flow–induced erosion of soft cohesive sediment beds. J. Geophys. Res.: Oceans 117 (C10). https://doi.org/10.1029/2012JC008072.

Wu, X., Bi, N., Yuan, P., Li, S., Wang, H., 2015. Sediment dispersal and accumulation off the present huanghe (Yellow River) delta as impacted by the water-sediment regulation scheme. Continent. Shelf Res. 111, 126–138. https://doi.org/10.1016/j.csr.2015.11.003.

Xie, W., He, Q., Wang, X., Guo, L., Zhang, K., 2018. Role of mudflat-creek sediment exchanges in intertidal sedimentary processes. J. Hydrol. 567, 351–360. https://doi.org/10.1016/j.jhydrol.2018.10.027.

Xie, W., He, Q., Zhang, K., Guo, L., Wang, X., Shen, J., Cui, Z., 2017. Application of terrestrial laser scanner on tidal flat morphology at a typhoon event timescale. Geomorphology 292, 47–58. https://doi.org/10.1016/j.geomorph.2017.04.034.

Xie, W., Sun, J., Guo, L., Xu, F., Wang, X., Ji, H., Fan, Y., Wang, Z.B., He, Q., 2023. Distinctive sedimentary processes on two contrasting tidal flats of the Yellow River Delta [Original Research]. Front. Mar. Sci. 10. https://doi.org/10.3389/fmars.2023.1259081.

Xie, W., Wang, X., Guo, L., He, Q., Dou, S., Yu, X., 2021. Impacts of a storm on the erosion process of a tidal wetland in the Yellow River Delta. Catena 205, 105461. https://doi.org/10.1016/j.catena.2021.105461.

Xue, C., 1993. Historical changes in the Yellow River Delta, China. Mar. Geol. 113 (3), 321–330. https://doi.org/10.1016/0025-3227(93)90025-Q.

Yang, S., Friedrichs, C.T., Shi, Z., Ding, P., Zhu, J., Zhao, Q., 2003. Morphological response of tidal marshes, flats and channels of the Outer Yangtze River mouth to a major storm. Estuaries 26 (6), 1416–1425. https://doi.org/10.1007/BF02803650.

Yang, W., Sun, T., Yang, Z., 2016. Effect of activities associated with coastal reclamation on the macrobenthos community in coastal wetlands of the Yellow River Delta, China: a literature review and systematic assessment. Ocean Coast Manag. 129, 1–9. https://doi.org/10.1016/j.ocecoaman.2016.04.018.

Yang, Z., Ji, Y., Bi, N., Lei, K., Wang, H., 2011. Sediment transport off the Huanghe (Yellow River) delta and in the adjacent Bohai Sea in winter and seasonal comparison. Estuar. Coast Shelf Sci. 93 (3), 173–181. https://doi.org/10.1016/j.ecss.2010.06.005.

Yao, R., Cai, L., Liu, J., Zhou, M., 2020. GF-1 satellite observations of suspended sediment injection of Yellow River estuary, China. Rem. Sens. 12 (19).

Zhang, X., Yang, Z., Zhang, Y., Ji, Y., Wang, H., Lv, K., Lu, Z., 2018. Spatial and temporal shoreline changes of the southern Yellow River (huanghe) delta in 1976–2016. Mar. Geol. 395, 188–197. https://doi.org/10.1016/j.margeo.2017.10.006.

Zhou, Z., Wu, Y., Fan, D., Wu, G., Luo, F., Yao, P., Gong, Z., Coco, G., 2022. Sediment sorting and bedding dynamics of tidal flat wetlands: modeling the signature of storms. J. Hydrol. 610, 127913. https://doi.org/10.1016/j.jhydrol.2022.127913.

Zhu, Q., Li, P., Li, Z., Pu, S., Wu, X., Bi, N., Wang, H., 2021. Spatiotemporal changes of coastline over the Yellow River Delta in the previous 40 Years with optical and SAR remote sensing. Rem. Sens. 13 (10).

Zhu, Q., van Prooijen, B.C., Wang, Z.B., Ma, Y.X., Yang, S.L., 2016. Bed shear stress estimation on an open intertidal flat using in situ measurements. Estuarine. Coastal and Shelf Science 182, 190–201. https://doi.org/10.1016/j.ecss.2016.08.028.

Zhu, Q., Wiberg, P.L., 2022. The importance of storm surge for sediment delivery to microtidal marshes. J. Geophys. Res.: Earth Surf. 127 (9), e2022JF006612. https://doi.org/10.1029/2022JF006612.